

Mott correlated states in the underdoped two-dimensional Hubbard model: variational Monte Carlo versus a dynamical cluster approximation.

Luca F. Tocchio, Hunpyo Lee, Harald O. Jeschke, Roser Valentí, and Claudius Gros
*Institut für Theoretische Physik, Goethe-Universität Frankfurt,
Max-von-Laue-Straße 1, 60438 Frankfurt am Main*

(Dated: January 21, 2021)

We investigate the properties of the frustrated underdoped Hubbard model on the square lattice using two complementary approaches, the dynamical cluster extension of dynamical mean field theory, and variational Monte Carlo simulations of Gutzwiller-Jastrow wavefunctions with backflow corrections. We compare and discuss data for the energy and the double occupancies, as obtained from both approaches. At small dopings, we observe a rapid crossover from a weakly correlated metal at low interaction strength U to a non-Fermi liquid correlated state with strong local spin correlations. Furthermore, we investigate the stability of the correlated state against phase separation. We observe phase separation only for large values of U or very large frustration. No phase separation is present for the parameter range relevant for the cuprates.

PACS numbers: 71.10.Fd, 71.27.+a, 71.30.+h, 71.10.Hf

I. INTRODUCTION

The Hubbard model on the square lattice is a minimal model for describing electronic correlation. This model has played a central role for the study of high- T_C superconductivity, since it is believed to capture the essential physics of the copper-oxygen planes in cuprate materials. Furthermore, the properties of the Hubbard model in the underdoped regime, *i.e.* in the proximity of the Mott insulating state at half-filling, is a stimulating research area due to the challenge in describing the physics of the correlated pseudogap state and its non-Fermi liquid behavior. Significant achievements in this field have been made, for instance, by the cluster extensions of dynamical mean-field theory¹⁻⁷, by means of a phenomenological theory⁸ and of the Gutzwiller approximation⁹, as well as on the basis of increasingly accurate variational wave functions^{10,11}.

Recently, it has been proposed that the pseudogap and the superconducting phases present at finite doping¹²⁻¹⁴ and for onsite U values corresponding to a Mott insulating state at half filling, can be continuously connected to a pseudogap and a superconducting phase at half-filling for U values lower than the critical U_c corresponding to the Mott-Hubbard metal-insulator transition (MIT). This proposal contrasts with Anderson's concept of superconductivity as a state emerging out of a Resonant Valence Bond (RVB) state¹⁵, a prototypical Mott-insulating state at half filling in the absence of magnetic order.

Another interesting feature of a correlated electron state in the underdoped regime is the tendency of the system to phase separate into an undoped state with strong antiferromagnetic correlations and a hole-doped region. Indeed, if the Hubbard model would be unstable to phase separation, its validity as a model to properly describe the development of superconductivity could be questioned. Phase separation occurs when the stability condition $\partial^2 E(n)/\partial n^2 > 0$ is violated, *i.e.* when the ground-state energy $E(n)$, as a function of electronic den-

sity n , is not any more convex. As introduced by Emery *et al.*¹⁶, phase separation can be studied by looking at the hole energy $E_\delta(\delta)$, defined as,

$$E_\delta(\delta) = \frac{E(\delta) - E(0)}{\delta} \quad (1)$$

where $\delta = 1 - n$ is the hole density. If the hole energy has a minimum at a critical doping δ_c , the system is unstable to phase separation for $\delta < \delta_c$. A difficulty when using the Emery criterion (1) is its strong dependence on the accuracy in the estimate of the ground state energy, as discussed in Ref. 17. In particular, less accurate ground state energies tend to overestimate the critical δ_c below which the system exhibits phase separation. This is a consequence of the fact that good estimates for the energy of low-doping states are hard to obtain because of the strong local correlations. Different approaches have led in the past to contradictory results for the Hubbard model in the parameter range relevant for hole-doped cuprates, ranging from absence of phase separation to a range of estimates for phase separation up to 10% doping¹⁸⁻²⁴. For the $t - J$ model²⁵⁻²⁸, *i.e.* for the large- U limit of the Hubbard model, phase separation is present at all dopings for large values of J , but the possible occurrence of phase separation close to half filling for small values of J has been a long-standing debate²⁶⁻²⁸.

In this work, we make use of variational Monte Carlo (VMC) simulations, including backflow correlations²⁹, and the dynamical cluster approximation (DCA)^{30,31} to address the properties of the Hubbard model on the square lattice with nearest and next-nearest neighbor hoppings in the underdoped regime both at zero and finite temperature. As already pointed out in Ref. 11, we distinguish a weakly correlated metal at small U (*i.e.* continuously connected to a half-filled metallic regime) and a strongly correlated state at intermediate to large U (*i.e.* when the half-filled case is insulating). We find significant differences between the two regimes in the static and in the dynamical spin correlations as well as in

the low-energy part of the self-energy. The above observations obtained from two complementary approaches, VMC and DCA, and the violation of the Luttinger sum rule for the strongly correlated state reported in a previous study¹¹, hint to a non-Fermi liquid nature of the strongly correlated state. The two states are separated by a crossover line at the critical interaction U_c , that may evolve into a first-order transition⁶ when doping is vanishing.

Moreover, we investigate the occurrence of phase separation in the underdoped Hubbard model. We find no tendency to phase separation when the Coulomb repulsion U is slightly above the critical U_c , regardless of the ratio t'/t between next-nearest and nearest neighbor hoppings, t' and t respectively. Our results therefore indicate that for intermediate values of the Coulomb repulsion ($U/t \sim 6 - 8$), the Hubbard model is stable against phase separation, irrespective of the value of t'/t . The actual value of t'/t is sensitive to the details of the high- T_c cuprate compound investigated and can be calculated, for example, in density functional theory, leading to $t'/t \simeq [-0.1, -0.4]$. A larger degree of frustration has been shown to correlate, in general, with higher critical temperatures³³.

If we increase the electron repulsion U at constant t'/t , the system is, in contrast, found to be unstable towards phase separation. However, since increasing the variational accuracy tends to suppress phase separation, we cannot exclude that an even more accurate approach could eliminate or significantly reduce the tendency to phase separate also for larger values of the Coulomb repulsion.

The paper is organized as follows: in Section II, we introduce the Hamiltonian and describe the VMC and the DCA approaches; in Section III, we compare ground-state energy and the density of double occupancies within the two methods, in Section IV, we discuss the non-Fermi liquid properties of the underdoped region at $U > U_c$, in contrast with the weakly correlated metal at $U < U_c$. In Section V the occurrence of phase separation is discussed and finally we present our conclusions in Section VI.

II. MODEL AND METHODS

We consider the frustrated Hubbard model with extended hopping on a two-dimensional square lattice,

$$\mathcal{H} = -t \sum_{\langle ij \rangle \sigma} c_{i\sigma}^\dagger c_{j\sigma} - t' \sum_{\langle\langle ij \rangle\rangle \sigma} c_{i\sigma}^\dagger c_{j\sigma} + \text{H.c.} + U \sum_i n_{i\uparrow} n_{i\downarrow}, \quad (2)$$

where $c_{i\sigma}^\dagger$ ($c_{i\sigma}$) denotes the electron creation (annihilation) operator of one electron on site i with spin $\sigma = \uparrow, \downarrow$, $\langle ij \rangle$ and $\langle\langle ij \rangle\rangle$ indicate nearest and next-nearest neighbor sites respectively; $n_{i\sigma} = c_{i\sigma}^\dagger c_{i\sigma}$ is the electron density; t and t' are the nearest and next-nearest neighbor hopping amplitudes, and U is the on-site Coulomb repulsion.

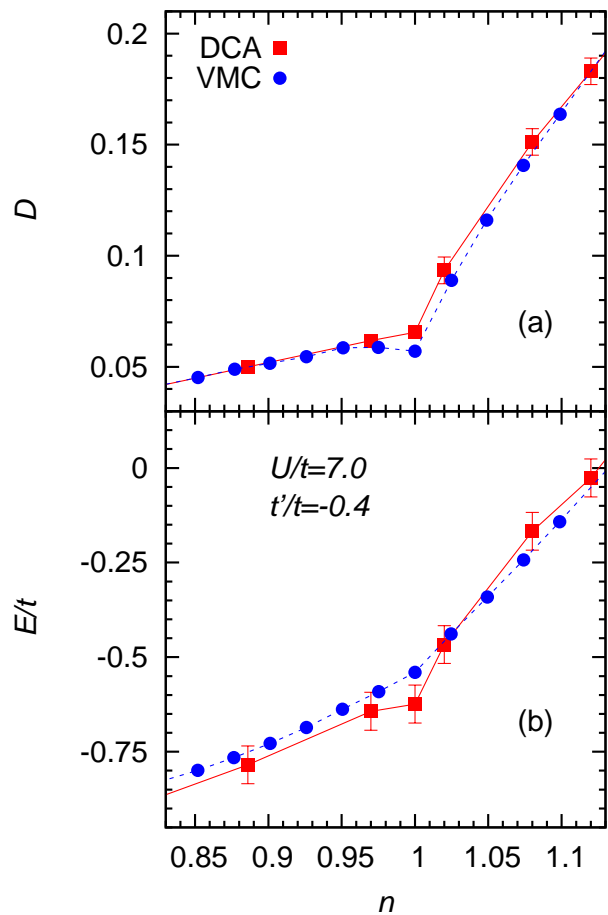


FIG. 1. (Color online) (a) Double occupancy D and (b) energy as a function of electronic density n for $U/t = 7.0$ and $t' = -0.4t$. Results are obtained using a VMC approach on an $L = 162$ lattice size (blue circles) and within DCA by means of a 2×2 plaquette in k -space for a temperature $T/t = 0.05$ (red squares). Errors in VMC are smaller than the symbol size. Lines are just guides to the eye.

A. Variational Monte Carlo

Variational Monte Carlo (VMC) simulations allow to perform non-perturbative calculations at zero temperature for one- and two-dimensional correlated and frustrated systems. VMC simulations are based on numerically sampling expectation values over a variational estimate of the ground-state wave function. Here we will use a powerful variational *ansatz* for frustrated electron systems which has been strictly tested by comparing extensively to analytical and numerical exact limiting cases. Our variational *ansatz* has been tested in particular against Bethe *ansatz* predictions for the Luttinger liquid exponents in one dimension³⁴, with respect to Lanczos results, in terms of wave function overlap, for a two-dimensional 18 site cluster³², and with respect to the results of density matrix renormalization group studies, in terms of the ground-state energy, for the 1D $J_1 - J_2$

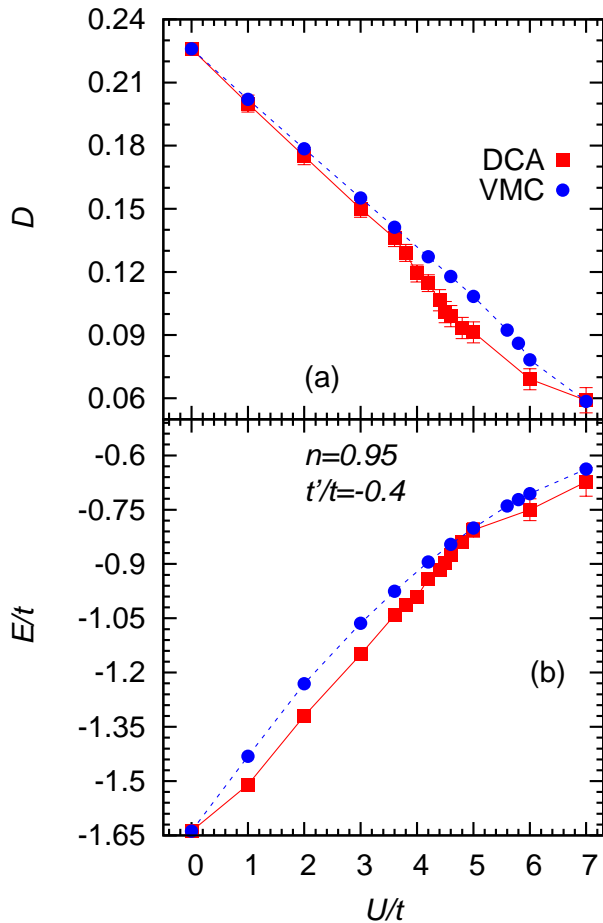


FIG. 2. (Color online) (a) Double occupancy D and (b) energy as a function of U/t for electron density $n = 0.95$ and $t' = -0.4t$. Data are obtained by a VMC approach on an $L = 162$ lattice size (blue circles) and within DCA by means of a 2×2 plaquette in k -space for a temperature $T/t = 0.05$ (red squares). Errors in VMC are smaller than the symbol size. Lines are just guides to the eye.

model²⁹.

The variational *ansatz* consists of three components. In a first step, we construct uncorrelated non-magnetic wave functions given by the ground state $|\text{BCS}\rangle$ of a superconducting Bardeen-Cooper-Schrieffer (BCS) Hamiltonian^{35–37}:

$$\mathcal{H}_{\text{BCS}} = \sum_{k\sigma} \xi_k c_{k\sigma}^\dagger c_{k\sigma} + \sum_k \Delta_k c_{k\uparrow}^\dagger c_{-k\downarrow}^\dagger + \text{H.c.}, \quad (3)$$

where both the free-band dispersion ξ_k and the pairing amplitudes Δ_k are variational functions. We use the parametrization

$$\begin{aligned} \xi_k &= -2\tilde{t}(\cos k_x + \cos k_y) - 4\tilde{t}' \cos k_x \cos k_y - \mu \quad (4) \\ \Delta_k &= 2\Delta_{\text{BCS}}(\cos k_x - \cos k_y), \quad (5) \end{aligned}$$

where the effective hopping amplitude \tilde{t} , the effective chemical potential μ , and the local pairing field Δ_{BCS}

are variational parameters to be optimized in order to minimize the variational energy. The parameter \tilde{t} is kept fixed to set the energy scale. We point out that large electronic correlations, as in proximity of a Mott insulator, lead to a strong renormalization of \tilde{t} with respect to the bare Hamiltonian value t' , see Ref. 11.

The correlated state $|\Psi_{\text{BCS}}\rangle$, without backflow terms, is then given by $|\Psi_{\text{BCS}}\rangle = \mathcal{J}|\text{BCS}\rangle$, where $\mathcal{J} = \exp(-1/2 \sum_{ij} v_{ij} n_i n_j)$ is a density-density Jastrow factor (including the on-site Gutzwiller term v_{ii}), with the v_{ij} 's being optimized for every independent distance $|i - j|$. Notably, within this kind of wave function, it is possible to obtain a pure (*i.e.*, non-magnetic) Mott insulator for a sufficiently singular Jastrow factor $v_q \sim 1/q^2$ (where v_q is the Fourier transform of v_{ij}), while a superconducting (metallic) state is found whenever $v_q \sim 1/q$ and $\Delta_{\text{BCS}} > 0$ ($\Delta_{\text{BCS}} = 0$)³⁴.

A size-consistent and efficient way to further improve the correlated state $|\Psi_{\text{BCS}}\rangle$ for large on-site interactions is based on backflow correlations. In this approach, each orbital that defines the unprojected state $|\text{BCS}\rangle$ is taken to depend upon the many-body configuration, in order to incorporate virtual hopping processes²⁹, in particular the recombination of neighboring charge fluctuations is favored. This is a substantial improvement with respect to Jastrow factors, where electron-electron correlation is included only via a multiplicative term. All results presented here are obtained by fully incorporating the backflow corrections and optimizing individually³⁸ every variational parameter in ξ_k and Δ_k , in the Jastrow factor \mathcal{J} , as well as for the backflow corrections. Calculations are performed on 45° tilted clusters with $L = 162$ lattice sites and periodic boundary conditions.

B. Dynamical Cluster Approximation

DCA is the cluster extension of single-site dynamical mean field theory (DMFT)³⁹, which includes, to a certain degree, momentum dependencies. Since the hopping matrix for sites within the considered cluster and for sites on different clusters is the same, in contrast to the cellular DMFT approach⁴⁰, the DCA self-consistent equation can be written in momentum space with the assumption that the self-energy is constant in the Brillouin zone sectors that are considered. The DCA self-consistency equation is given as

$$\bar{G}_\sigma(\mathbf{K}, i\omega_n) = \frac{1}{N} \sum_{\tilde{\mathbf{K}}} \frac{1}{i\omega_n + \mu - \epsilon_{\mathbf{K}+\tilde{\mathbf{K}}} - \Sigma_\sigma(\mathbf{K}, i\omega_n)}, \quad (6)$$

where N is the number of k points in each Brillouin zone sector (compare Figure 3), μ the chemical potential, \mathbf{K} is the cluster momentum, $\epsilon_{\mathbf{K}+\tilde{\mathbf{K}}}$ the dispersion relation, ω_n are the fermionic Matsubara frequencies, and where the summation over $\tilde{\mathbf{K}}$ is performed in each Brillouin zone sector. In our calculations, we employed the DCA cluster with $N_c = 4$, where $\mathbf{K} = (0, 0), (0, \pi), (\pi, 0)$, and

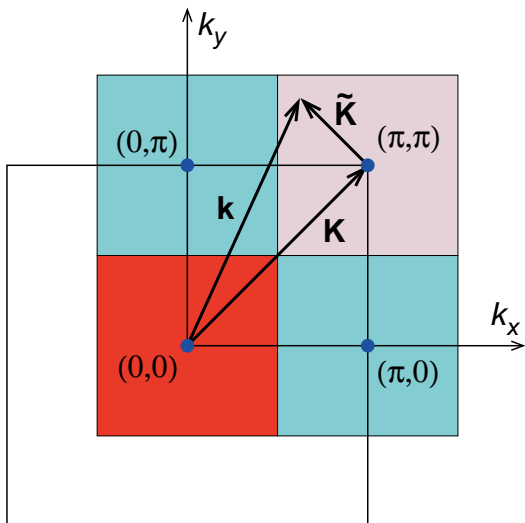


FIG. 3. Partitioning of the square lattice Brillouin zone within the $N_c = 4$ DCA method. There are four sectors characterized by the cluster momentum \mathbf{K} . An arbitrary reciprocal space vector \mathbf{k} is represented as a sum of \mathbf{K} and a vector $\tilde{\mathbf{K}}$ running within the cell labeled by \mathbf{K} .

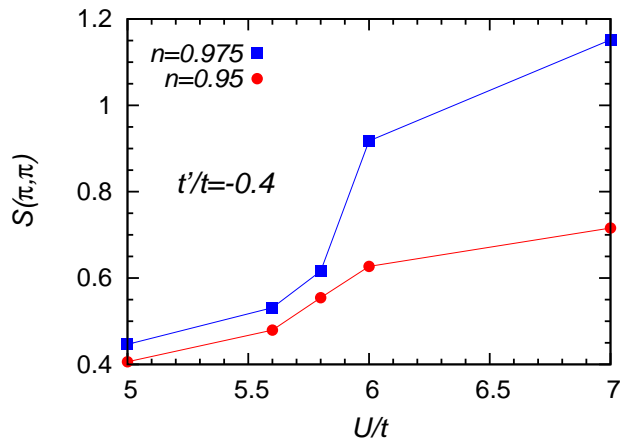


FIG. 4. (Color online) Evolution of the static structure factor correlations $S(q) = \langle s_{-q}s_q \rangle$ at $Q = (\pi, \pi)$ as a function of U/t for $n = 0.975$ (blue squares) and $n = 0.95$ (red circles) at $t'/t = -0.4$. The appearance of the non-FL region is characterized by a rapid increase in the short-range antiferromagnetic correlations. Data are obtained by means of VMC simulations on an $L = 162$ lattice size.

(π, π) . The converged self-energy $\Sigma_\sigma(\mathbf{K}, i\omega_n)$ is evaluated by means of Eq. (6) and the Dyson equation. We employ the interaction expansion continuous-time quantum Monte Carlo approach as an impurity solver^{41,42}. All calculations presented here are for a temperature $T/t = 0.05$ and we perform more than 10^7 QMC samplings for the impurity Green's function $G(i\omega_n)$, in order to keep the QMC statistical errors smaller than 5×10^{-3} for the first Matsubara frequency. As the Matsubara frequencies increase, the error bar decreases.

III. ENERGY AND DOUBLE OCCUPANCIES

In Fig. 1, we compare the average number of double occupancies per site $D = \langle n_{i,\uparrow}n_{i,\downarrow} \rangle$ and the energy, for $U/t = 7.0$ and $t' = -0.4t$ as a function of the electron density n , as obtained from VMC and DCA simulations. For the DCA calculations, the energy is calculated by

$$E = \frac{T}{N} \sum_{n,\mathbf{k},\sigma} [\epsilon_{\mathbf{k}} \bar{G}_\sigma(\mathbf{k}, i\omega_n)] e^{i\omega_n 0^+} + UD, \quad (7)$$

where the index \mathbf{k} runs over the first Brillouin zone and we considered the asymptotic behavior of the self-energy in the limit of large Matsubara frequencies $i\omega_n$: $\Sigma_\sigma(\mathbf{K}, i\omega_n) \sim U^2 n_\sigma (1 - n_\sigma) / i\omega_n$. The error Δ_n of the self-energy $\Sigma(i\omega_n)$ is calculated by

$$\Delta_n = \frac{2\xi}{G(i\omega_n)^2}, \quad (8)$$

where $i\omega_n$ is the Matsubara frequency and ξ is the error of $G(i\omega_n)$; it turns out that Δ_n is almost constant as a function of n . The error on the energy is then estimated as the difference between the energy calculated in Eq. (7) by using $\Sigma(i\omega_n) + \Delta_n$ as the self-energy and the energy calculated by using $\Sigma(i\omega_n) - \Delta_n$ as the self-energy.

For the large value of U/t presented in Fig. 1, both approaches show good agreement in the double occupancy and in the energy, even if the energies in DCA are characterized by large error bars, due to the high-frequency tail of the self-energy.

In Fig. 2, we present the double occupancy D and the energy close to half filling, for $n = 0.95$ and $t' = -0.4t$, as a function of the interaction strength U/t . We observe that the results for the double occupancies at strong coupling ($U/t \sim 7.0$) and at weak coupling ($U/t < 3.5$) are in good agreement but they differ in the range $U/t = 4 - 6$. This discrepancy is related to the fact that VMC and DCA predict different values for the location of U_c/t of the metal-insulator transition at half-filling. The singlet RVB state is dominant in the DCA on a 2×2 cluster, thus favoring correlated states, and also the VMC results can be slightly dependent on the accuracy of the trial wave function. The metal-insulator transition at half-filling, which is weakly first-order, takes place at $U_c/t = 5.8 \pm 0.2$ within VMC¹¹, while for DCA, on a 2×2 cluster, the critical U_c/t is approximately estimated at $U_c/t = 4.6 \pm 0.4$ ^{13,44}. Note that the metal-insulator transition in VMC has been determined by looking at the static structure factor $N(q) = \langle n_{-q}n_q \rangle$, where $n_q = 1/\sqrt{L} \sum_{r,\sigma} e^{iqr} n_{r,\sigma}$ is the Fourier transform of the particle density. Indeed, the metallic phase is characterized by $N(q) \sim q$ for $q \rightarrow 0$, which implies a vanishing gap for particle-hole excitations. On the contrary, in the insulating phase, $N(q) \sim q^2$ for $q \rightarrow 0$, implying the fact that the charge gap is finite.

At difference with the double occupancies, the energy data do not show in general good agreement within the

two methods. One possible reason for the discrepancy is that the energy in DCA is calculated in terms of the self-energy, see Eq. 7, that is taken as constant within the Brillouin zone sectors. This means that we cannot obtain a true k -dependent self-energy in our small cluster DCA calculations. Furthermore, the high-frequency part of the self-energy is evaluated according to an approximate formula that may introduce a further systematic error in the calculated self-energy. Also VMC energies are not exact and further improvements in the wave function may lower the variational energy.

Signatures of the metal-insulator transition occurring at half filling are visible at low doping in VMC calculations, where both the double occupancy D and the energy show kinks for interactions U close to the critical U_c . Similar signatures are more difficult to infer from the DCA data around $U/t = 4.5$ due to the larger error bars, but can be clearly observed in the behavior of the one-particle self-energy, as we discuss in the next section. In fact, both approaches, irrespective of the actual location of the MIT predicted in each method, exhibit a rapid crossover between a weak-coupling Fermi-liquid (FL) and an intermediate to large U non-FL regime for small but finite dopings. This conclusion will be discussed in the next section, based on the observed behavior of the one-particle self-energy and of the two-particle correlation functions.

IV. NON-FERMI LIQUID VS. FERMI LIQUID PROPERTIES

In this Section, we explore in more detail the FL and non-FL properties of the frustrated Hubbard model close to half filling, using both the VMC and DCA approaches. Long-range static correlations can be evaluated within VMC but not within DCA, due to cluster-size restrictions. Dynamical quantities like the one-particle self-energy can however be calculated within DCA and not with VMC; the two approaches complement each other nicely.

The nature of the non-Fermi liquid region has been characterized, using VMC simulations¹¹, by a strong renormalization of the underlying Fermi surface and a small violation of the Luttinger sum rule. Here, we assess the magnetic properties at low dopings via the static structure factor, defined as

$$S(q) = \frac{1}{L} \sum_{m,n} e^{iq(R_m - R_n)} \langle S_m^z S_n^z \rangle, \quad (9)$$

where S_m^z is the z -component of the spin operator on site m and where L denotes the total number of sites. The presence of (short-range) antiferromagnetic correlations is signaled by the appearance of a (non-diverging) peak in $S(q)$, located at $Q = (\pi, \pi)$.

As shown in Fig. 4, for the two electron densities $n = 0.975$ and $n = 0.95$ at $t'/t = -0.4$, the non-Fermi

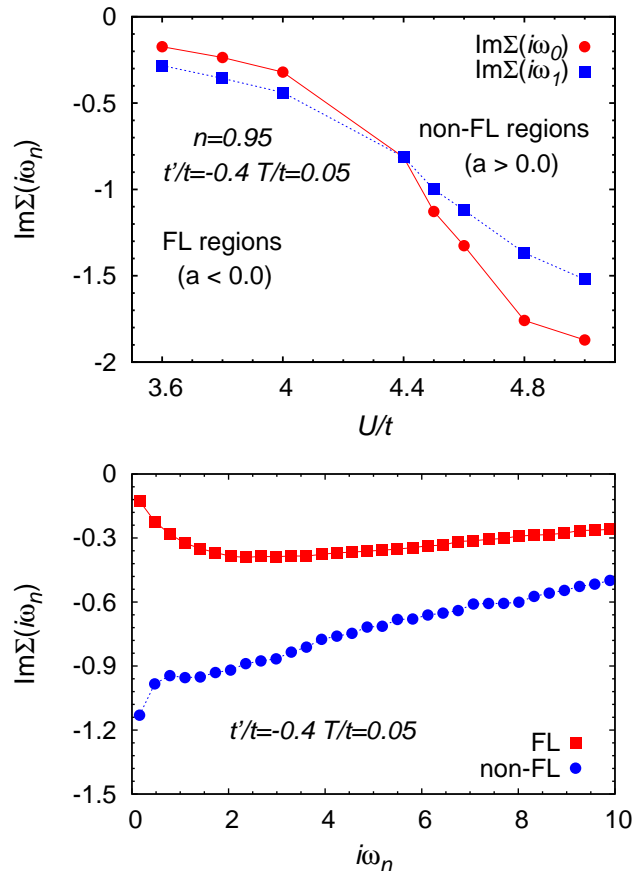


FIG. 5. (Color online) Upper panel: The imaginary part of the lowest (red circles) and the second lowest (blue squares) self-energy values in Matsubara frequencies as a function of U/t at $T/t = 0.05$ with $n = 0.95$ and $t' = -0.4t$. Data have been obtained by DCA using a 2×2 cluster. The crossing point of both self-energies occurs around $U/t = 4.5$, which is the same critical U_c/t where the kink in the double occupancy data of Fig. 2 is located. The quantity a is defined in Eq. (10). Lower panel: The imaginary part of the self energy as a function of the Matsubara frequencies at $U/t = 3.6$ and $n = 0.94$ (FL, red squares) and at $U/t = 5.0$ and $n = 0.96$ (non-FL, blue circles). Data have been obtained by DCA using a 2×2 cluster.

liquid state at $U/t \gtrsim 6$ is characterized by antiferromagnetic correlations which are substantially enhanced with respect to the weakly correlated metallic phase at $U/t \lesssim 6$. For the smaller doping, $n = 0.975$, the two regimes are clearly separated by a rapid increase in the value of $S(Q)$, which could be compatible with a first-order transition, while for the larger doping the jump is less evident and the observed rise in the strength of the short-ranged spin-spin correlations is more in agreement with a smooth crossover.

Next, we plot the imaginary part of the lowest and the second lowest Matsubara frequency self-energy values as a function of U/t at $T/t = 0.05$, $n = 0.95$ and $t' = -0.4t$

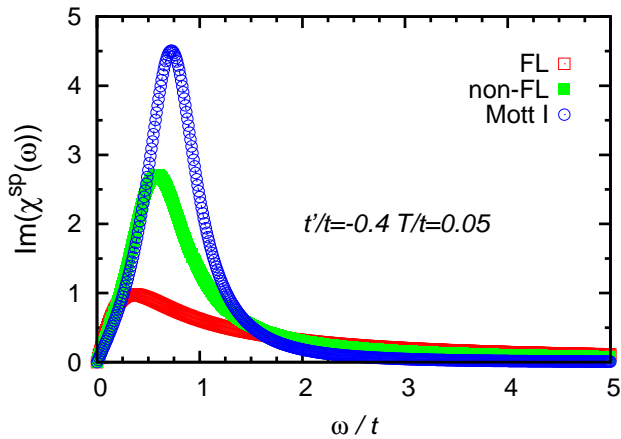


FIG. 6. (Color online) The local dynamical spin susceptibility $\text{Im}(\chi^{\text{sp}}(\omega))$ for $U/t = 3.6$ and $n = 0.94$ (FL, open red squares), $U/t = 5.0$ and $n = 0.96$ (non-FL, filled green squares) and $U/t = 7.0$ and $n = 1.0$ (Mott insulator, open blue circles), as a function of the real frequency ω/t at $T/t = 0.05$ and $t' = -0.4t$. A Padé approximation has been employed for the analytical continuation of $\chi^{\text{sp}}(\tau)$.

(see Fig. 5, upper panel), obtained using DCA. We define

$$a = \frac{\text{Im}(\Sigma(i\omega_1)) - \text{Im}(\Sigma(i\omega_0))}{\omega_1 - \omega_0}, \quad (10)$$

where $\text{Im}(\Sigma(i\omega_0))$ is the imaginary part of the lowest Matsubara frequency self-energy value and $\text{Im}(\Sigma(i\omega_1))$ is the imaginary part of the second lowest Matsubara self-energy value. Negative ratios $a < 0$ indicate (quasi)-FL behavior, while positive ratios $a > 0$ suggest a non-Fermi liquid state. Indeed, the value of the imaginary part of the self-energy converges to zero (or to small values due to the effect of temperature) for $i\omega_n \rightarrow 0$ in the Fermi-liquid regime, while it is monotonically decreasing for $i\omega_n \rightarrow 0$ in the non-Fermi liquid state, see Fig. 5, lower panel. From the data presented in Fig. 5, we find a critical $U_c/t = 4.5$ between FL and non-FL states, which is in agreement with the location of the small kink in the double occupancy D , compare Fig. 2.

Finally, we present in Fig. 6 the local dynamical spin susceptibility $\text{Im}(\chi^{\text{sp}}(\omega))$ obtained within DCA with 10^8 QMC samplings, by performing the analytical continuation of

$$\chi^{\text{sp}}(\tau) = \langle S^z(\tau)S^z(0) \rangle, \quad (11)$$

where $S^z = \frac{1}{2}(n_\uparrow - n_\downarrow)$ and τ is the imaginary time, with the help of the Padé approximation. The $\text{Im}(\chi^{\text{sp}}(\omega))$ around $\omega/t = 0.5$ is strongly suppressed in the FL region at $U/t = 3.6$ and $n = 0.94$. This low-frequency peak is dominant in the non-FL region at $U/t = 5.0$ and $n = 0.96$ and in the Mott insulating region at $U/t = 7.0$ and $n = 1$. We relate the enhancement of the low-energy peak in non-FL and Mott insulator regions to the formation of short-range antiferromagnetic correlations, as presented

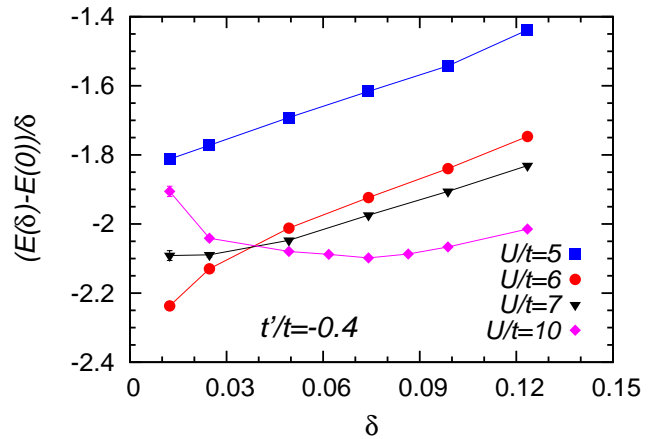


FIG. 7. (Color online) The hole energy $E_\delta(\delta) = (E(\delta) - E(0))/\delta$ as a function of doping for different values of U/t at $t'/t = -0.4$. Data are obtained by means of VMC simulations on an $L = 162$ lattice size

in Fig. 4, in terms of increased RVB-type singlet pairing. These results demonstrate the complementarity of the DCA and VMC methods in identifying the region of possible non-FL behavior and they are compatible with studies of the Kagome and the triangular lattice^{45,46}.

V. PHASE SEPARATION

We investigate now the possible occurrence of phase separation in the hole-doped regime $n < 1$, by considering the hole energy defined in Eq. (1). The system is unstable to phase separation for $\delta < \delta_c$, if the hole energy has a minimum at a critical doping δ_c , while a monotonically increasing hole energy corresponds, on the other hand, to an energetically favorable homogeneous solution for the doping levels investigated. Physically, phase separation is driven by magnetic correlations, which can be substantially increased, in the phase without holes, at the expense of the kinetic energy.

In Fig. 7, we focus on the case $t'/t = -0.4$, and vary the interaction strength U/t . As expected, we find that no phase separation is possible when the half-filled case is metallic ($U/t = 5$), due to the absence of a relevant magnetic energy scale. Phase separation is also not observed, interestingly, when U is only slightly above the critical interaction U_c ($U/t = 6$, in Fig. 7), at least for small but finite doping levels $\delta \gtrsim 0.02$. At very low dopings $\delta \lesssim 0.02$ (and $U/t = 7$) phase separation could possibly be present. However, since the model is expected to exhibit a magnetic instability close to half-filling, a possible phase separation occurring for $\delta \lesssim 0.02$ would be masked by long-range magnetic order. For larger values of U/t phase separation seems however to be energetically favorable for a wider range $\delta \lesssim 0.08$ of doping levels. The data for larger electron repulsion ($U/t \sim 20$) are

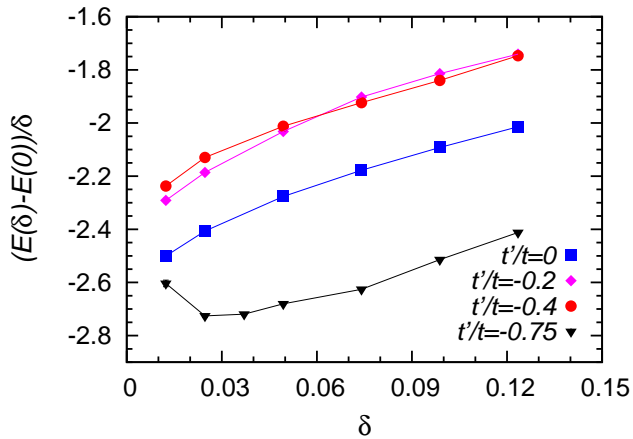


FIG. 8. (Color online) The hole energy $E_\delta(\delta) = (E(\delta) - E(0))/\delta$ as a function of doping for the four cases $U/t = 6, t'/t = 0$ (blue squares), $U/t = 6, t'/t = -0.2$ (pink diamonds), $U/t = 6, t'/t = -0.4$ (red circles) and $U/t = 8, t'/t = -0.75$ (black triangles). The data has been obtained by means of VMC simulations on an $L = 162$ lattice.

not shown in Fig. 7, but they exhibit trends similar to the case $U/t = 10$. However, we cannot exclude that better estimates of the ground-state energy can reduce this tendency to phase separate, as detailed in Ref. 17. This is a consequence of the fact that good estimates for the energy of low-doping states are hard to obtain because of the strong local correlations.

In Fig. 8, we show the hole energy as a function of doping for four values of the next-nearest neighbor hopping, ranging from $t'/t = 0$ to $t'/t = -0.75$. The value of the Coulomb repulsion is slightly above the critical U_c , that is located between $U/t = 5$ and $U/t = 6$ for $-0.4 < t'/t < 0$, while it is located between $U/t = 7$ and $U/t = 8$ at $t'/t = -0.75$. In all the cases relevant for the cuprates, $t'/t \simeq [-0.1, -0.4]$, no phase separation occurs. Only in a small range $\delta \lesssim 0.02$ a tendency for phase separation is observed for $t'/t = -0.75$. Thus, our data suggest that for the cuprates the Hubbard model is not unstable against phase separation when the value of the electronic repulsion is chosen to be close to the critical interaction U_c of the Mott-Hubbard transition.

VI. CONCLUSIONS

When investigating correlated electron systems numerical or analytical approximations are generically necessary and the accuracy of the employed approach is notoriously difficult to control. Here we compare results obtained by two complementary approaches, DCA and VMC. We find good agreement for the calculation of the double occupancies, apart from the value of the critical Hubbard- U for the Mott-Hubbard metal-insulator transition at half filling, while comparing energies is more problematic, as discussed in Sec. III. We use the complementary information, static long-range correlations provided by VMC and dynamical properties provided by DCA, to investigate the physics at finite but low doping levels. We find that the crossover from a weakly correlated electron state at intermediate to small values of U to a non-Fermi liquid state at intermediate to large values of U is characterized by a strong increase in local magnetic correlations. In this respect, we do not find evidence for non-Fermi liquid properties below the critical Hubbard- U , as suggested instead by a recent DCA study^{12,13}. Our result is a solid feature of the VMC approach¹¹. The application of DCA in the present work has been oriented to supplement the dynamical properties that are missing in VMC and we do not exclude that other studies within DCA can show evidence of non-Fermi liquid properties also below the critical U , though this is in contradiction with VMC. This remains a controversial issue^{13,47} and needs further study. In Sec. V, we investigate the stability of the non-Fermi liquid state against phase separation and find it to be stable for all parameters relevant for the cuprates. These studies further prove the synergies obtainable when using complementary methods for the study of frustrated and correlated electron systems.

ACKNOWLEDGMENTS

We would like to thank the Deutsche Forschungsgemeinschaft for financial support through grants SFB/TR49 (L.F.T.) and FOR 1346 (H.L.), and the Helmholtz association for financial support through grant HA216/EMMI (H.O.J.). L.F.T. thanks Federico Becca for useful discussions.

¹ M. Civelli, M. Capone, S. S. Kancharla, O. Parcollet, and G. Kotliar, Phys. Rev. Lett. **95**, 106402 (2005).

² S. Sakai, Y. Motome, and M. Imada, Phys. Rev. Lett. **102**, 056404 (2009).

³ M. Civelli, Phys. Rev. B **79**, 195113 (2009).

⁴ E. Khatami, K. Mikelsons, D. Galanakis, A. Macridin, J. Moreno, R. T. Scalettar, and M. Jarrell, Phys. Rev. B **81**, 201101(R) (2010).

⁵ E. Gull, M. Ferrero, O. Parcollet, A. Georges, and A. J. Millis, Phys. Rev. B **82**, 155101 (2010).

- ⁶ G. Sordi, K. Haule, and A.-M. S. Tremblay, *Phys. Rev. B* **84**, 075161 (2011).
- ⁷ A. Liebsch and N.-H. Tong, *Phys. Rev. B* **80**, 165126 (2009).
- ⁸ K.-Y. Yang, T. M. Rice, and F.-C. Zhang, *Phys. Rev. B* **73**, 174501 (2006).
- ⁹ R. S. Markiewicz, J. Lorenzana, G. Seibold, and A. Bansil, *Phys. Rev. B* **81**, 014509 (2010).
- ¹⁰ R. Sensarma, M. Randeria, and N. Trivedi, *Phys. Rev. Lett.* **98**, 027004 (2007).
- ¹¹ L. F. Tocchio, F. Becca, and C. Gros, *Phys. Rev. B* **86**, 035102 (2012).
- ¹² M. Sentef, P. Werner, E. Gull, and A. P. Kampf, *Phys. Rev. Lett.* **107**, 126401 (2011).
- ¹³ E. Gull, O. Parcollet, and A. J. Millis, arXiv:1207.2490 (unpublished).
- ¹⁴ G. Sordi, P. Sémon, K. Haule, and A.-M. S. Tremblay, *Phys. Rev. Lett.* **108**, 216401 (2012).
- ¹⁵ P. W. Anderson, *Science* **235**, 1196 (1987).
- ¹⁶ V. J. Emery, S. A. Kivelson, and H. Q. Lin, *Phys. Rev. Lett.* **64**, 475 (1990).
- ¹⁷ F. Becca, M. Capone, and S. Sorella, *Phys. Rev. B* **62**, 12700 (2000).
- ¹⁸ A. Macridin, M. Jarrell, and Th. Maier, *Phys. Rev. B* **74**, 085104 (2006).
- ¹⁹ M. Aichhorn, E. Arrighoni, M. Potthoff, and W. Hanke, *Phys. Rev. B* **76**, 224509 (2007).
- ²⁰ C.-C. Chang and S. Zhang, *Phys. Rev. B* **78**, 165101 (2008).
- ²¹ K.-S. Chen, S. Pathak, S.-X. Yang, S.-Q. Su, D. Galanakis, K. Mielson, M. Jarrell, and J. Moreno, *Phys. Rev. B* **84**, 245107 (2011).
- ²² S. Y. Chang, S. Pathak, and N. Trivedi, *Phys. Rev. A* **85**, 013625 (2012).
- ²³ K.-S. Chen, Z. Y. Meng, T. Pruschke, J. Moreno, and M. Jarrell, *Phys. Rev. B* **86**, 165136 (2012).
- ²⁴ S. Watanabe and M. Imada, *J. Phys. Soc. Jpn.* **73**, 1251 (2004).
- ²⁵ R. Valentí and C. Gros, *Phys. Rev. Lett.* **68**, 2402 (1992).
- ²⁶ M. Lugas, L. Spanu, F. Becca, and S. Sorella, *Phys. Rev. B* **74**, 165122 (2006).
- ²⁷ P. Corboz, S. R. White, G. Vidal, and M. Troyer, *Phys. Rev. B* **84**, 041108 (2011).
- ²⁸ W.-J. Hu, F. Becca, and S. Sorella, *Phys. Rev. B* **85**, 081110(R) (2012).
- ²⁹ L. F. Tocchio, F. Becca, and C. Gros, *Phys. Rev. B* **83**, 195138 (2011).
- ³⁰ M. H. Hettler, A. N. Tahvildar-Zadeh, M. Jarrell, T. Pruschke, and H. R. Krishnamurthy, *Phys. Rev. B* **58**, 7475(R) (1998).
- ³¹ T. Maier, M. Jarrell, T. Pruschke, and M. Hettler, *Rev. Mod. Phys.* **77**, 1027 (2005).
- ³² L. F. Tocchio, F. Becca, A. Parola, and S. Sorella, *Phys. Rev. B* **78**, 041101(R) (2008).
- ³³ E. Pavarini, I. Dasgupta, T. Saha-Dasgupta, O. Jepsen, and O. K. Andersen, *Phys. Rev. Lett.* **87**, 047003 (2001).
- ³⁴ M. Capello, F. Becca, S. Yunoki, M. Fabrizio, and S. Sorella, *Phys. Rev. B* **72**, 085121 (2005).
- ³⁵ C. Gros, *Phys. Rev. B* **38**, 931(R) (1988).
- ³⁶ F. C. Zhang, C. Gros, T. M. Rice, and H. Shiba, *Supercond. Sci. Technol.* **1**, 36 (1988).
- ³⁷ C. Gros, *Annals of Physics* **189**, 53 (1989).
- ³⁸ S. Yunoki and S. Sorella, *Phys. Rev. B* **74**, 014408 (2006).
- ³⁹ A. Georges, G. Kotliar, W. Krauth, and M. J. Rozenberg, *Rev. Mod. Phys.* **68**, 13 (1996).
- ⁴⁰ G. Kotliar, S. Y. Savrasov, G. Palsson, and G. Biroli, *Phys. Rev. Lett.* **87**, 186401 (2001).
- ⁴¹ A. N. Rubtsov, V. V. Savkin, and A. I. Lichtenstein, *Phys. Rev. B* **72**, 035122 (2005).
- ⁴² E. Gull, A. J. Millis, A. I. Lichtenstein, A. N. Rubtsov, M. Troyer and P. Werner, *Rev. Mod. Phys.* **83**, 349 (2011).
- ⁴³ E. Gull, P. Werner, A. Millis, and M. Troyer, *Phys. Rev. B* **76**, 235123 (2007).
- ⁴⁴ E. Gull, P. Werner, X. Wang, M. Troyer, and A. J. Millis, *Europhys. Lett.* **84**, 37009 (2008).
- ⁴⁵ B. Kyung, *Phys. Rev. B* **75**, 033102 (2007).
- ⁴⁶ T. Ohashi, N. Kawakami, and H. Tsunetsugu, *Phys. Rev. Lett.* **97**, 066401 (2006).
- ⁴⁷ S. Dayal, R. T. Clay, and S. Mazumdar, *Phys. Rev. B* **85**, 165141 (2012).